# Supplementary data

# Ordered Mesoporous nZVI/Zr-Ce-SBA-15 Catalysts Used for Nitrate Reduction: Synthesis, Optimization and Mechanism

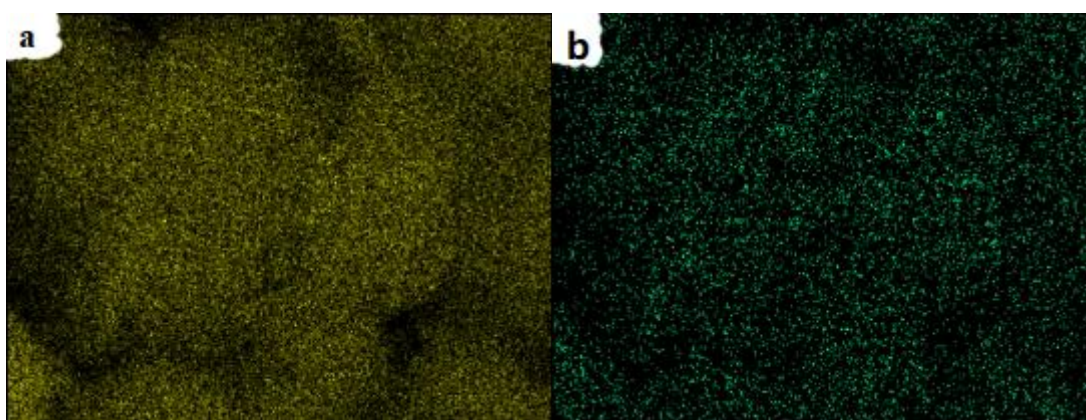Ruimin Zhang [1,*], Haixia Liu [1], Weili Jiang [2], Weijing Liu [2]

**Figure S1.** SEM characterization of Si (**a**) and Zr (**b**) distribution of nZVI/Zr-Ce-SBA-15 composites.
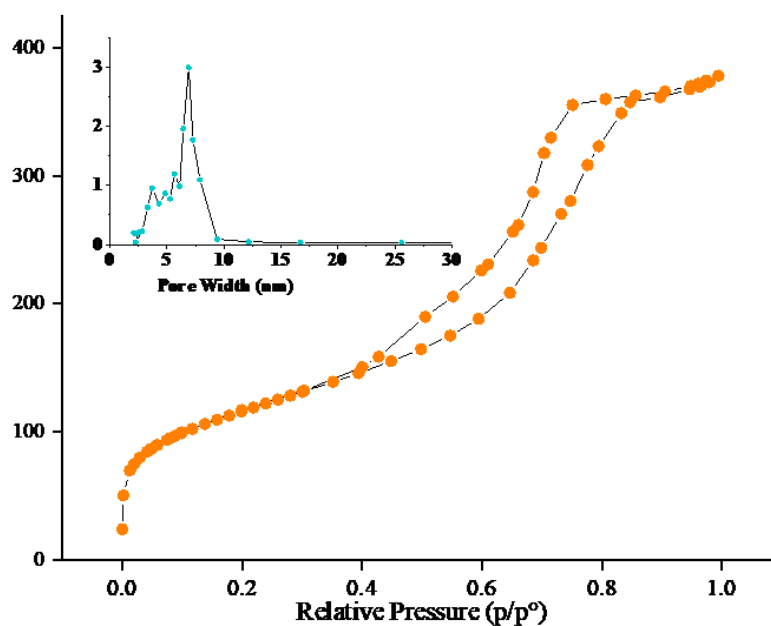
**Figure S2.** Characterization of N$_2$ adsorption for nZVI/Zr-Ce-SBA-15 composites.
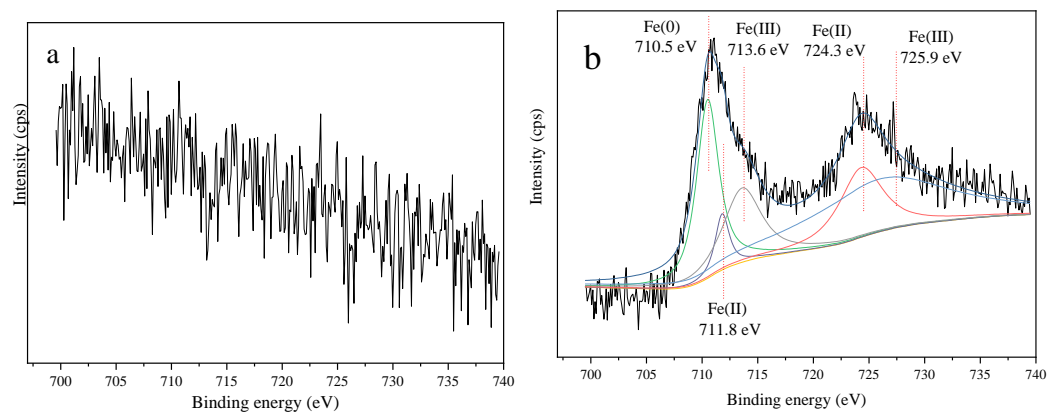
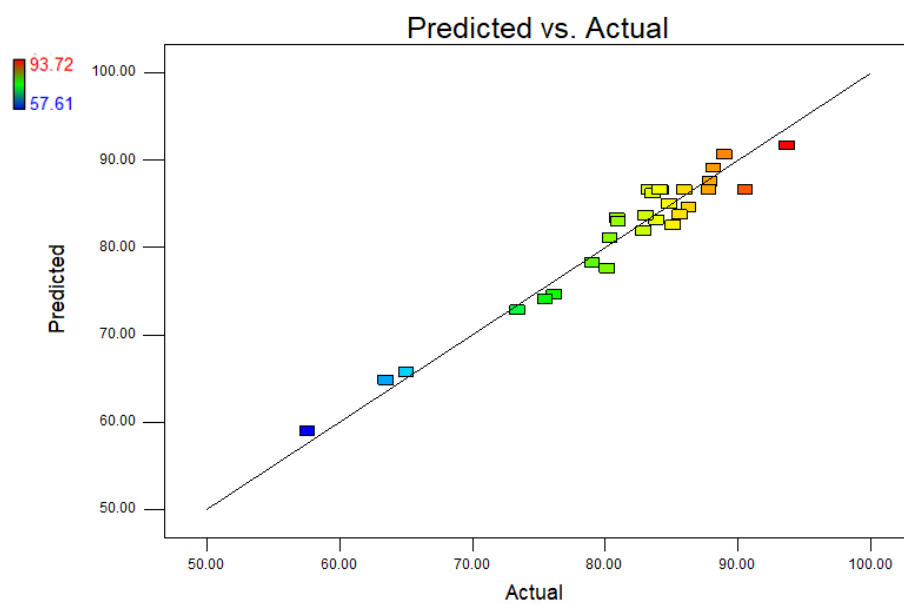**Figure S3.** XPS characterization of magnified Fe2p spectrogram of Zr-Ce-SBA-15 (**a**) and nZVI/Zr-Ce-SBA-15 (**b**).
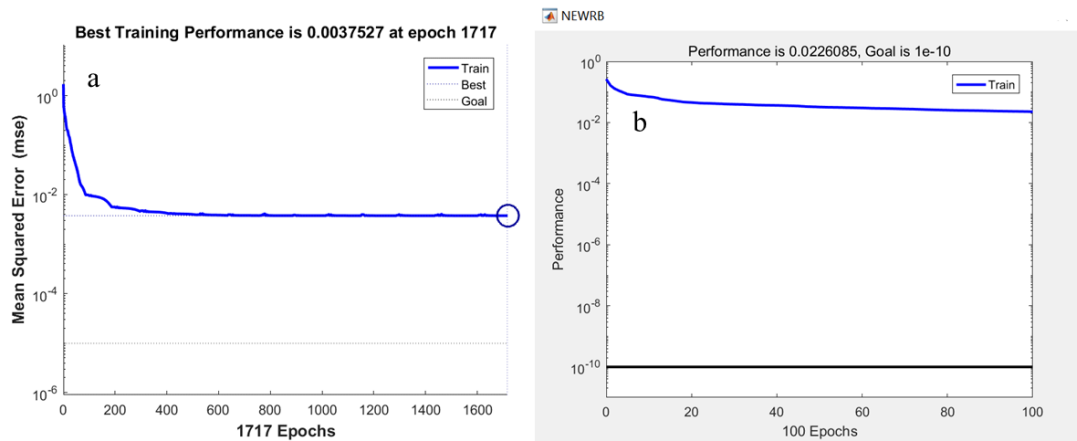


**Figure S4**. Comparison with the predicted and actual values.

**Figure S5.** The training performance of ANN (**a**) and RBFNN (**b**).
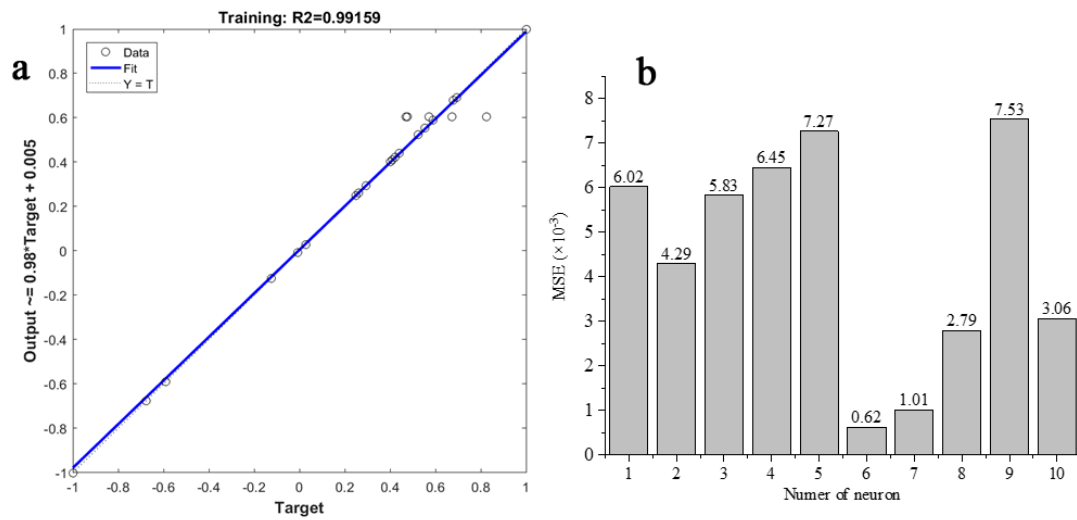


**Figure S6.** The correlation coefficient between target and output values (**a**) and the lowest MSE value (**b**) in ANN model.
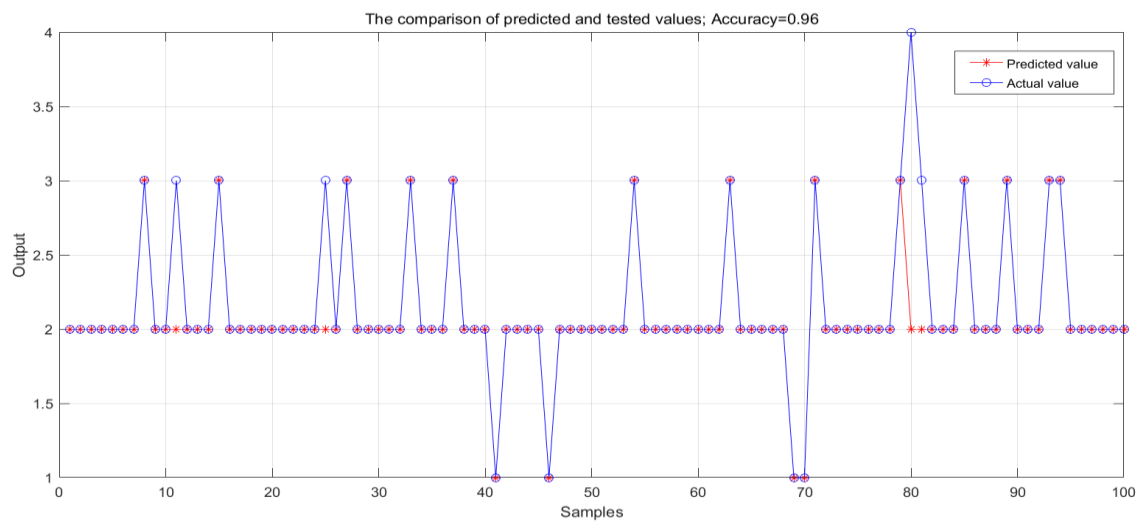


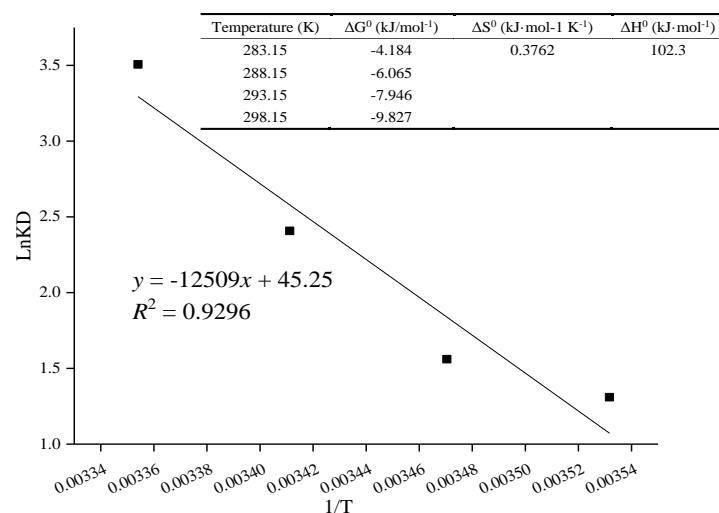**Figure S7.** The comparison of predicted and actual values by RBFNN.

| Temperature (K) | $\Delta G^0$ (kJ/mol$^{-1}$) | $\Delta S^0$ (kJ·mol-1 K$^{-1}$) | $\Delta H^0$ (kJ·mol$^{-1}$) |
|---|---|---|---|
| 283.15 | -4.184 | 0.3762 | 102.3 |
| 288.15 | -6.065 | | |
| 293.15 | -7.946 | | |
| 298.15 | -9.827 | | |

$y = -12509x + 45.25$

$R^2 = 0.9296$

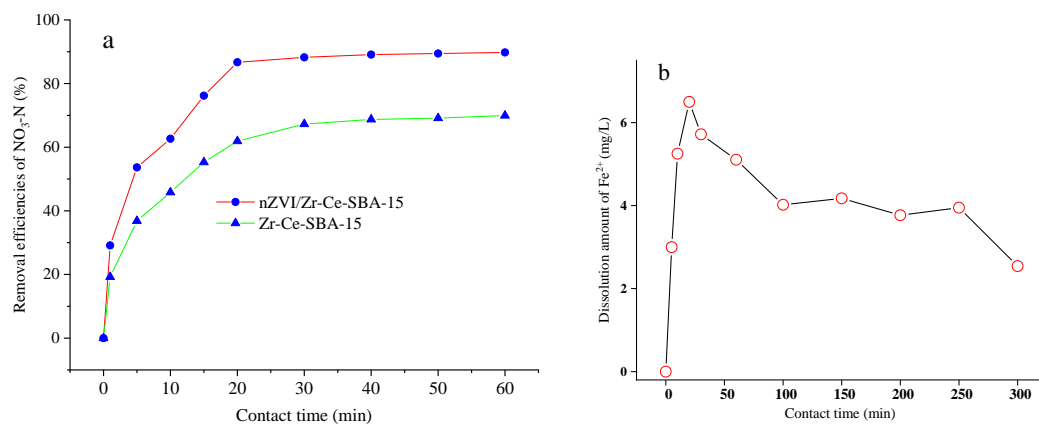**Figure S8.** The fitting process and parameters of thermodynamics.



**Figure S9.** The comparison of removal efficiency of NO$_3$-N using Zr-Ce-SBA-15 and nZVI/Zr-Ce-SBA-15 composites (**a**) and Fe$^{2+}$ dissolution of nZVI/Zr-Ce-SBA-15 in solution (**b**) (Zr-Ce-SBA-15 or nZVI/Zr-Ce-SBA-15 = 0.15 g; initial NO$_3$-N concentration = 60 mg/L and initial pH = 4; temperature=25 ℃).
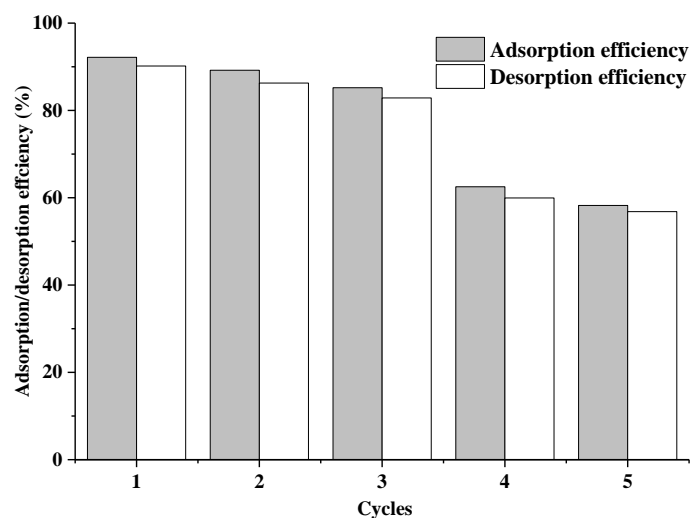


**Figure S10.** The adsorption and desorption efficiencies of nZVI /Ce-Zr-SBA-15.